Spring 4-30-2016

Ultracold Trimer Ion Formation of Rb and K

Michael Cantara
University of Connecticut - Storrs, michael.cantara@uconn.edu

Ultracold Trimer Ion Formation of Rb and K

Michael Cantara

A paper submitted in partial fulfillment of the requirements for
the University of Connecticut Honors Scholar and University
Scholar Programs in Physics
May 2016

ACKNOWLEDGEMENTS

During my studies at the University of Connecticut I have benefited from exceptional mentorship through the physics department. I would like to offer my sincerest gratitude to Dr. William Stwalley for providing years of education, support and opportunies both in laboratory work and in building a theoretical foundation for my AMO physics knowledge. I am indebted to Dr. Ed Eyler for not only teaching four of my courses, but for also helping me learn the hands-on aspects of experimental physics both in his lab-based courses and in his own lab. I am grateful to Dr. Phil Gould for many fruitful discussions in ultracold physics in lab group meetings.

I am also incredibly grateful to my adviser for three years of theoretical particle physics research, Dr. Peter Schweitzer. I was first introduced to physics research by Dr. Schweitzer, and with his immense help I was able to co-author a publication. His patience and knowledge have served to provide an incredible foundation for my research career.

I cannot thank Dr. Ryan Carollo, Dr. Jen Carini, Scott Galica and Dr. Yoann Bruneau enough for their support and patience in the laboratory, and for always supporting my broader education in AMO physics.

Lastly, I would like to thank Dr. Gerald Dunne for providing extraordinary guidance and insight with the graduate application process.

TABLE OF CONTENTS

LIST OF FIGURES

1. INTRODUCTION

The cooling of molecules into the ultracold regime allows for high resolution laser spectroscopy that reveals their complex rotational and vibrational structure [1]. As the temperature is lowered towards absolute zero, the kinetic energy of the particles approaches zero, and therefore the Doppler shift approaches zero. With the Doppler shift negligibly small, spectral resolution is now primarily limited by the natural linewidth of the molecular peaks. Ultracold molecules produced through photoassociation typically reside in high-lying vibrational states. Further, ultracold temperatures make possible the production of atoms or molecules that will reside in the lowest few states of the system. The high population in a few select states provides stronger and less congested spectra compared to in uncooled systems. Interactions with the system, such as photoassociation, are well defined in ultracold systems and populate select states that are easily observable. With the control allowed by ultracold temperatures we are able to observe quantum mechanical phenomena that are otherwise hidden from view.

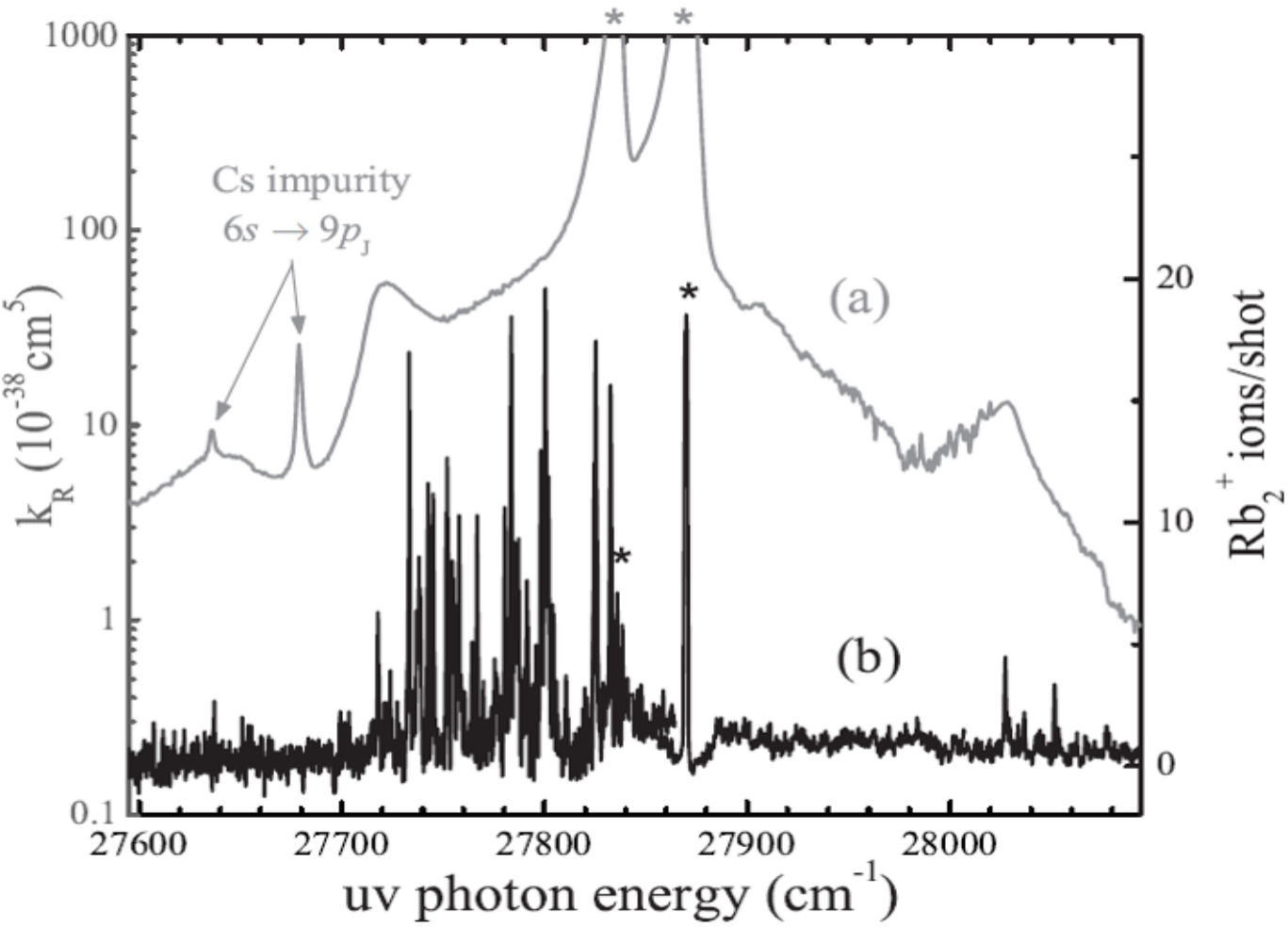

Fig. 1.1: (From [2]) Rb_2 spectra in a heat-pipe oven (a) contrasted with spectra taken at ultracold temperatures of ~ 120 μK (b). The free–bound absorption and pressure broadening that dominate in (a) are minimal in (b), allowing the features of the very few rotational levels of Rb_2 populated in (b) to be resolved.

1.1 Recent Developments

In 1995 Eric Cornell and Carl Wieman were the first to experimentally produce gaseous Bose-Einstein condensate at the University of Colorado at Boulder NIST-JILA lab [3]. By cooling a gas of rubidium atoms to 170 nanokelvin, they were able to condense the bosonic atoms into the lowest accessible quantum state. This new form of matter, though extremely fragile to maintain, has allowed physicists to explore fundamental questions such as wave-particle duality via interference between condensates, superfluidity, and the slowing of light through electromagnetically induced transparency. Just as laser light separates itself from ordinary light by consisting of photons that are of the same frequency and direction, the uniqueness of Bose-Einstein condensate comes from the fact that the atoms in this state of matter are identical. This attribute allows for high levels of control over atoms limited only by the uncertainty principle itself. This control will ultimately allow highly precise measurements and instruments that will likely play a significant role in our future.

Superfluidity, a state of matter related to Bose-Einstein condensation, was first discovered in helium when it was cooled below a critical temperature of 2.17 K. Below this temperature a massive leap in heat capacity occurs, the density of the helium drops, and a portion of the atoms form a Bose-Einstein condensate and are thus in the lowest possible energy level. The helium atoms that form the BEC are observed to have zero viscosity and thus possess unique physical characteristics, including the ability to self-propel and defy gravity as well as surface tension. The behavior of superfluids is described by quantum mechanics, and as such they have become a common example of quantum mechanical behavior on the macroscopic scale.

The atom laser was first experimentally realized in 1996 by Professor Wolfgang Ketterle of MIT [3]. The atom laser has an output of a matter wave, or a beam of atoms, which is both coherent and bright. Like an optical laser, an atom laser can be highly focused and can be collimated to travel great distances without spreading. In a typical gas, atoms fill many modes of the system when they scatter. However, when a Bose-Einstein condensate is formed, it causes stimulated scattering of atoms into the condensate. The atoms will reside mainly in one mode of the system, the lowest energy state, and will mimic optical lasers when appropriately emitted from the trap. Several notable differences distinguish atom lasers from their optical counterpart:

- The number of atoms in an atom laser are not amplified– instead, the number of atoms in the ground state increases while the population of other states decreases.
- Atom lasers will interact with other atoms, and therefore atom lasers cannot travel far in air.
- Atom lasers consist of massive particles and therefore are subject to a gravitational force.
- The van der Waals interaction of atoms with surfaces makes atomic mirrors difficult to construct, although atom optical elements can be realized through the use of lasers and magnetic fields.

Though the atom laser is relatively young, its potential to be implemented in experiments requiring high levels of control is evident. Where the optical laser allows for high precision in light-matter interactions, the atom laser will allow for new levels of manipulation and control in matter-matter interactions of the future.

Optical lattices are constructed by counter-propagating laser beams which provide periodic potential wells within which neutral atoms may be trapped and cooled. The potential wells are produced by the Stark shift in the atoms of the lattice, which results from the conservative interaction of the incoming laser light with the induced dipole moment of the atoms. The optical lattice is rather easily modified, with changes in the laser power resulting in changes in the well depth of the lattice while adjustments in laser frequency or the relative angle between the counter-propagating beams will result in a change in periodicity. Due to their freedom from defects, their ability to be easily manipulated and their close resemblance to crystal lattices, optical lattices have been used to investigate band structure, e.g. Bloch oscillations as well as Bragg scattering.

1.2 Future Applications

Gaining a deeper understanding of the inner structure of molecules will enhance applications such as quantum information science and the measurement of fundamental physical constants. Already, quantum computers are being used in testing newly developed software for vulnerabilities, and in the near future will solve problems in mathematics and engineering ranging from prime factorization to many-body systems. Optical frequency combs, developed in molecular physics labs, have the ability to determine, in real-time, molecular species at the parts-per-billion level. Such devices are capable of serving as quality control and environmental safety tools to detect concentrations of greenhouse gases such as methane, carbon dioxide and nitrous oxide, pollutants such as isoprene and formaldehyde, and even methanol and ethane, which are found in

human breath, all with unsurpassed precision [4]. In the rapidly expanding field of optical communications, each data transmitting channel currently requires its own laser to operate. Frequency combs generated by microresonators, capable of relatively large powers and repetition rates, could provide an immense advantage by supporting hundreds of telecommunication channels from a single laser.

Lastly, quantum simulations such as the trapped-ion simulator built by NIST in 2012 will have a great impact on future studies of physics [5]. Such experiments are able to control interactions between hundreds of qubits. With such control, the complex computations involved in the numerous quantum mechanical interactions of low temperature physics and of high temperature superconductors may be realized. Quantum simulation attempts to investigate quantum behavior that would prove too difficult to study in the laboratory through the use of laser pulses causing qubits to interact. The system is engineered so that the behavior of the simulator and the behavior of the actual experiment are identical. Thus, quantum simulations provide experimental results that are currently impossible to obtain in the laboratory. As more simulations are constructed, physics that has proven elusive in the laboratory will enter the realm of observable.

2. PHOTOASSOCIATION AND SPECTROSCOPY

The process where an electronically excited molecule is formed by the collision of two free atoms and the absorption of light is known as photoassociation. The formation of a molecule typically occurs near the Condon point, R_c. At this internuclear separation the photon energy is equal to the energy difference between the excited and ground states [6]. A photoassociation spectrum displays the number of molecules produced as a laser traverses a range of frequencies. In many PA spectra of alkali metals Doppler broadening plays a minor role because transitions often occur to short-lived states. With atoms prepared at ultracold temperatures the range of initial kinetic energies is similar to the natural linewidth of the excited molecular state because thermal broadening is minimal. Therefore, the photoassociation of alkali metals provides high resolution spectra with linewidths only marginally larger than the natural linewidths. A further benefit of PA spectroscopy is that it naturally lends itself to producing molecules in high vibrational levels. These long range molecules contain atoms whose wavefunctions are nearly undistorted interacting with electrostatic forces such as van der Waals and dipole-dipole that depend solely on the properties of the atoms. PA spectroscopy has led to the accurate measurement of radiative lifetimes for alkali metal atoms and provides binding energies relative to atomic asymptotes without requiring the extrapolation required in higher temperature bound-bound molecular spectroscopy. Another advantage PA spectroscopy provides is

the ability to produce molecules in low rotational levels. Due to the rotational barrier, which is composed of both the centrifugal potential and the molecular binding potential, atoms are only able to reach short internuclear distances if they possess low levels of collisional angular momentum. As the collisional angular momentum of the atoms increases, the rotational barrier correspondingly increases and prevents the atoms from approaching small internuclear distances.

There are three widely used methods for detecting a PA spectrum. Trap loss spectroscopy, where the fluorescence of the cooled atoms is monitored as a laser is scanned through a frequency range, is a powerful technique for observing photoassociation [6]. When two atoms undergo photoassociation, they are able to radiatively decay back into two atoms: the atoms may be either hot, in which case they will be lost from the trap, or they may be cold, in which case there will be no loss from the trap. The two atoms may also radiatively decay from their bound state to a lower bound state, and the fluorescence of the atomic cloud will correspondingly decrease. Equation 2.1 summarizes the reaction where the excited molecule formed radiatively decays to two free atoms– whether the atoms are "hot" or "cold" depends on the energy of the photon emitted in the decay process. Equation 2.2 summarizes the reaction where the excited molecules radiatively decay to a lower bound state. Here the * represents an excited state of the molecule.

$$A + A + h\nu \rightarrow A_2^* \rightarrow A + A + h\nu' \tag{2.1}$$

$$A + A + h\nu \rightarrow A_2^* \rightarrow A_2 + h\nu'' \tag{2.2}$$

Another method that is currently employed in our laboratory and that has found widespread use elsewhere is the ionization de-

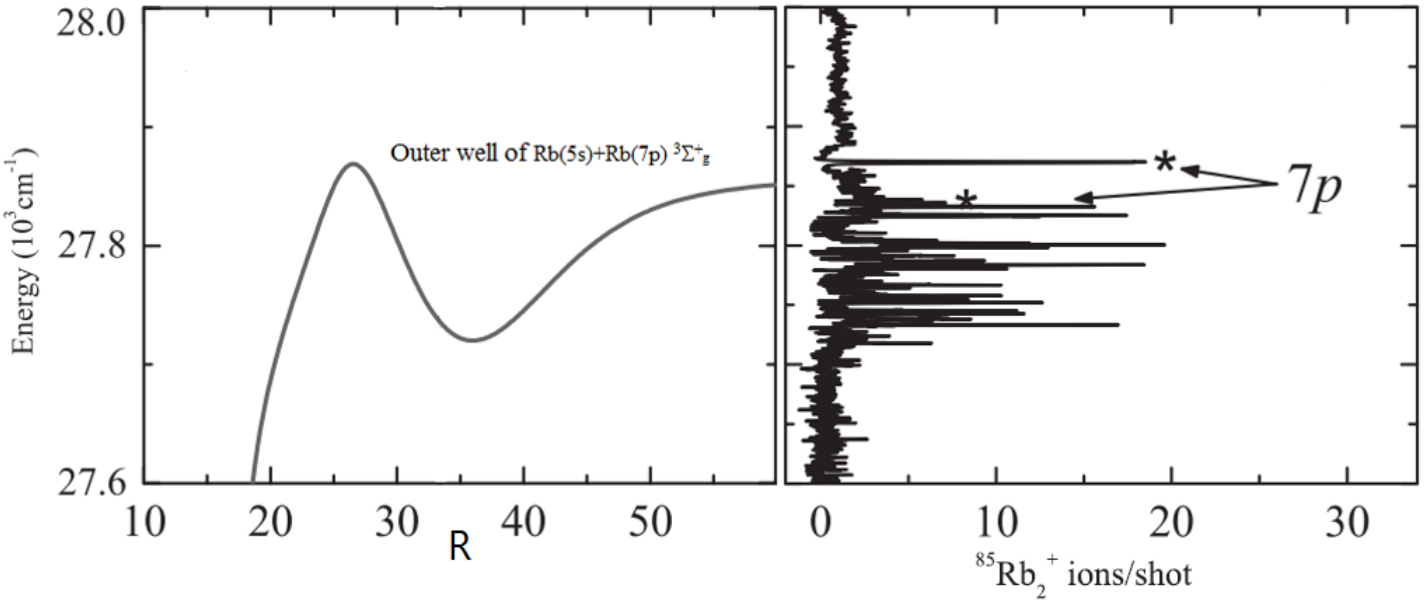

Fig. 2.1: (From [15, 16]) Left Panel: the outer well potential energy curve in units of Bohr radii of the $^3\Sigma_g^+$ state. Right Panel: Ionization detection of populated vibrational states in the $^3\Sigma_g^+$ state of Rb_2 near the Rb(7p) atomic limit.

tection scheme. After the excited molecule is formed via PA, and decays to a bound molecule (Eq. 2.2), a second laser proceeds to ionize the bound molecule. Using an ion detector to count the number of molecular ions, and thus the number of molecules produced, a PA spectrum is produced (Fig. 2.1).

The last method I will discuss occurs only in certain conditions where predissociation may occur. In predissociation the excited state molecule undergoes an electronic transition to a repulsive state, which will then decompose the molecule into a ground state and an excited state atom. Detection of the the excited state atom then allows for a PA spectrum to be constructed.

2.1 Rydberg Atoms and Molecules

A Rydberg atom is an atom of high principal quantum number n, and thus has an electronic wavefunction that is distant from the nucleus. In our laboratory we investigate Rydberg molecules, specifically the class known as trilobite molecules, in which a Rydberg atom is bound to a ground-state atom through the attractive potential that arises from the negative scattering length of the Rydberg electron from the ground-state atom [7]. Trilobite molecules are bound by a novel chemical bond that is distinct from ionic, covalent and van der Waals bonds [2]. Thus, the applications of trilobite molecules extend well beyond physics with exciting implications for ultracold exotic chemistry, materials engineering and quantum information science. To create, manipulate and resolve states in such exotic molecules, however, requires cooling into the ultracold regime and implementing high resolution laser spectroscopy that reveals their complex rotational and vibrational structure [6].

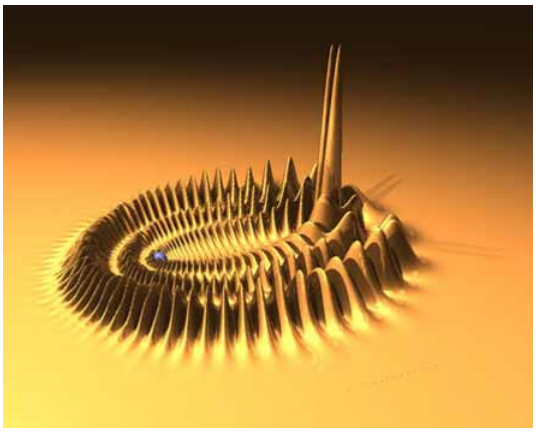

Fig. 2.2: (From [8]) The electronic wavefunction squared of a trilobite molecule. The small ball on the left represents the Rb^+ ionic Rydberg core and the electronic wavefunction possesses very strong peaking at the location of the ground state Rb atom.

3. THE MAGNETO-OPTICAL TRAP

The magneto-optical trap (MOT) is the favored instrumental technique for confining atoms and cooling them to less than 1 mK temperatures. Although for our present purposes ∼1 mK temperatures are sufficient, the MOT is also a common starting point for cooling atoms to the nanoKelvin regime for Bose-Einstein condensation, where evaporative cooling and other techniques are applied after the initial cooling provided by the MOT. The operation of the MOT relies on the Doppler shift and the Zeeman splitting of the energy levels of the atoms to be cooled.

The approach is to cool a sample of the atomic species by passing three pairs of counter-propagating laser beams through the chamber, which is at ultra-high vacuum to insure only the atomic species of interest is present and to prevent collisions with any background gases. The laser beams are red-detuned from the atomic resonance such that any atoms approaching a beam will see an upshifted frequency that is near atomic resonance. Thus, the atoms will absorb the photon and its corresponding momentum, and will slow down as a result of the velocity-dependent force from the lasers. Without a magnetic field, such a system is called an optical molasses. It is important to note that if an atom is traveling away from a beam, it will see a downshifted frequency that is even further from atomic resonance, and as a result has a low probability of absorbing such a photon, so the force from the light is minimal. The magneto part of the name stems from the spatially varying magnetic quadrupole

field generated by anti-Helmholtz coils. With such a field, the Zeeman effect will split the sublevels of the atoms and, as the atoms move away from the center of the chamber, this splitting will increase [9]. Thus, as atoms travel farther from the center of the trap, the atomic resonance will shift closer to the frequency of the incident laser beam and the atoms will have a greater probability of receiving a photon kick towards the center of the chamber. The spatial-dependence of the magnetic field combined with the MOT laser polarization serves to trap the atoms. Therefore the magnetic and optical fields serve to confine the atoms and cool the atoms, respectively.

Once the ultracold cloud of atoms is formed in the MOT, an optical dipole trapping scheme may be implemented to further cool the atoms and increase the atomic density.

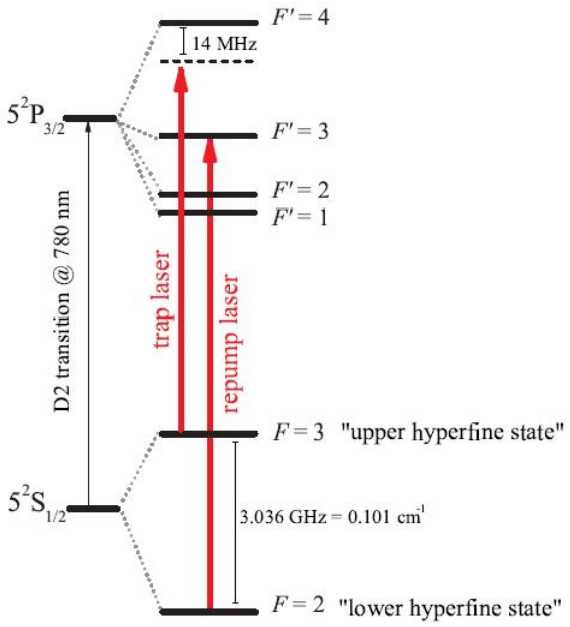

Fig. 3.1: (From [15]) Energy levels of $5^2S_{1/2}$ and $5^2P_{3/2}$, including hyperfine structure, used for the MOT transitions (red) of ^{85}Rb in our experiment.

4. THE OPTICAL DIPOLE TRAP

4.1 Introduction

Several techniques exist for producing atoms and molecules in the ultracold regime, including the magneto-optical trap discussed in the previous chapter. However, the optical dipole trapping scheme provides distinct advantages over the magneto-optical trap: optical dipole traps can utilize far-detuned laser light and thus optical excitations of the atoms are extremely low compared to the MOT. Also, higher densities are attainable with a dipole trap since the MOT produces light-assisted inelastic collisions which set a lower-bound to the atomic density [10].

The MOT, however, does possess a few key advantages over the the optical dipole trap, and by combining the two we can exploit the strengths of both systems while minimizing their respective weaknesses. Through its strong optical excitation of atoms, the MOT is able to cool atomic samples from thermal lab temperatures. The dipole trap operates through the much weaker mechanism of far-detuned light, and as such warm atoms easily escape from its weaker trapping potential. Thus the approach is to utilize the MOT to cool an ensemble of atoms at room temperature into the range of hundreds of microKelvin, then to make use of the optical dipole trapping scheme in order to confine the cooled atoms and increase the atomic density.

4.2 The Dipole Potential and Scattering Rate

The interaction of an atom with an incident light field can be shown to produce an optical dipole force that is nearly conservative. The force results from the redistribution of photons between the plane waves which together form the incident light wave through cycles of absorption and stimulated emission [11]. As such, a potential can be derived from the force that arises. It is the minima of this potential that are responsible for the trapping of atoms in an optical dipole trap.

4.2.1 Classical Oscillator Model

Here we consider a classical radiation field with an atom acting as a simple oscillator. The amplitude of the dipole moment, $\tilde{p}$, the amplitude of the electric field, $\tilde{E}$, and the complex polarizability, α, are related by the following equation:

$$\tilde{p} = \alpha \tilde{E}. \tag{4.1}$$

The potential of the induced dipole moment is then given by

$$U_{dipole} = -\frac{1}{2}\langle \vec{p} \cdot \vec{E} \rangle, \tag{4.2}$$

where $\vec{p}(\vec{r},t) = \hat{e}\, p(\vec{r}) e^{-i\omega t}$, $\vec{E}(\vec{r},t) = \hat{e}\, E(\vec{r}) e^{-i\omega t}$ and $\hat{e}$ is the unit polarization vector. Using the intensity relation $I = 2\epsilon_o c|E|^2$, and applying a factor of $\frac{1}{2}$ to account for the dipole moment being induced instead of permanent, we write

$$U_{dipole} = -\frac{\mathbf{Re}(\alpha)}{2\epsilon_0 c} I. \tag{4.3}$$

It is then straightforward to compute the optical dipole force:

$$F_{dipole}(\mathbf{r}) = -\nabla U_{dipole}(\mathbf{r}) = \frac{\mathbf{Re}(\alpha)}{2\epsilon_0 c}\nabla I(\mathbf{r}). \tag{4.4}$$

Next we look at the scattering rate, Γ_{sc}, which is related to the power absorbed by the atom acting as an oscillator, P_{abs}, and the frequency of the incident laser light, ω:

$$\Gamma_{sc} = \frac{P_{abs}}{\hbar\omega}. \tag{4.5}$$

The power absorbed by the oscillator is determined by

$$P_{abs} = \langle \dot{\mathbf{p}}\mathbf{E} \rangle = \frac{\omega}{\epsilon_0 c}\mathbf{Im}(\alpha) I. \tag{4.6}$$

Therefore the scattering rate may be written as

$$\Gamma_{sc}(\mathbf{r}) = \frac{\mathbf{Im}(\alpha)}{\hbar\epsilon_0 c} I(\mathbf{r}). \tag{4.7}$$

Consider the atom in the Lorentz model of a classical oscillator: an electron bound inelastically to the core has an oscillation eigenfrequency of ω_0 and emits dipole radiation that results in damping of its motion. The equation of motion for such a system is then given by

$$\ddot{x} + \Gamma_\omega \dot{x} + \omega_0^2 x = -\frac{e}{m_e} E(t), \tag{4.8}$$

where

$$\Gamma_\omega = \frac{e^2\omega^2}{6\pi\epsilon_0 m_e c^3} \tag{4.9}$$

is the classical damping rate resulting from radiative energy loss. A rearrangement of terms yields

$$\frac{e^2}{m_e} = \frac{6\pi\epsilon_0 c^3 \Gamma_\omega}{\omega^2}. \tag{4.10}$$

By integration of the equation of motion, the polarizability is determined:

$$\alpha = \frac{e^2}{m_e}\frac{1}{\omega_0^2 - \omega^2 - i\omega\Gamma_\omega}. \tag{4.11}$$

We now define the on-resonance damping rate term:

$$\Gamma \equiv \left(\frac{\omega_0}{\omega}\right)^2 \Gamma_\omega, \tag{4.12}$$

allowing us to rewrite the polarizablity as

$$\alpha = 6\pi\epsilon_0 c^3 \frac{\Gamma\omega_0^2}{\omega_0^2 - \omega^2 - i(\omega^3/\omega_0^2)\Gamma}. \tag{4.13}$$

In the case of dipole trapping with far-detuned light and low saturation, we have very low scattering rates: $\Gamma_{sc} \ll \Gamma$. Under this approximation we may write both the dipole potential and the scattering rate as follows:

$$U_{dipole}(\mathbf{r}) = -\frac{3\pi c^2}{2\omega_0^3}\xi I(\mathbf{r}) \tag{4.14}$$

and

$$\Gamma_{sc}(\mathbf{r}) = \frac{3\pi c^2}{2\hbar\omega_0^3}\left(\frac{\omega}{\omega_0}\right)^3 \xi^2 I(\mathbf{r}) \tag{4.15}$$

where $\xi = \left(\frac{\Gamma}{\omega_0-\omega} + \frac{\Gamma}{\omega_0+\omega}\right)$.
We now assume that the laser is tuned relatively near the atomic resonance ω_0. Defining the laser detuning as $\Delta \equiv \omega - \omega_0$, in the small detuning approximation we have

$$|\Delta| \ll \omega_0 \tag{4.16}$$

and

$$\frac{\omega}{\omega_0} \approx 1. \tag{4.17}$$

By using the rotating wave approximation, we may neglect terms containing $\frac{1}{\omega_0+\omega}$. Therefore, $\xi = \frac{\Gamma}{\Delta}$. Thus we arrive at general expressions for the dipole potential and the scattering rate:

$$U_{dipole}(\mathbf{r}) = \frac{3\pi c^2}{2\omega_0^3}\frac{\Gamma}{\Delta}I(\mathbf{r}) \tag{4.18}$$

and

$$\Gamma_{sc}(\mathbf{r}) = \frac{3\pi c^2}{2\hbar\omega_0^3}\left(\frac{\Gamma}{\Delta}\right)^2 I(\mathbf{r}) \tag{4.19}$$

From these two equations we can see that the dipole potential scales with I/Δ and the scattering rate scales with I/Δ^2. Experiments take advantage of such scaling by using a large laser detuning in combination with high intensity in order to minimize the scattering rate while still maintaining the required potential depth necessary to trap the atomic species of interest.

4.2.2 AC Stark Shift

A quantum mechanical treatment agrees well with the classically derived result and provides a more general set of equations. Second order perturbation theory for non-degenerate states yields the energy correction

$$\Delta E = \sum_{i\neq j}\frac{|\langle j|H|i\rangle|^2}{E_i^{(0)} - E_j^{(0)}} \tag{4.20}$$

Here, the interacting Hamiltonian, the light field, has the form

$$H = -\hat{\mu}\hat{\boldsymbol{E}} \tag{4.21}$$

where $\hat{\mu} = -e\boldsymbol{r}$. The zeroth order energies, $E^{(0)}$, may be determined by viewing the ground state and excited state through the dressed state picture. For the ground state, the energy of the system is contained purely within the incident light field whose energy is

given by $n\hbar\omega$, where n is the number of photons. When an atom absorbs one of the incident photons it is raised to a state of energy $\hbar\omega_o$, where ω_o is the frequency of the optical transition and depends on the atomic structure. The light field then has an energy given by $(n-1)\hbar\omega$. Therefore, we can write

$$E_i^{(0)} - E_j^{(0)} = (n\hbar\omega) - (\hbar\omega_o + (n-1)\hbar\omega) = \hbar\Delta, \tag{4.22}$$

where $\Delta \equiv \omega - \omega_o$. Therefore, if we assume a two level atom so that the summation is only over one term, the second order correction may be rewritten as follows:

$$\Delta E = \pm \frac{|\langle j|\hat{\mu}|i\rangle|^2}{\Delta} |E|^2, \tag{4.23}$$

where $+$ is for the ground state and $-$ for the excited state. Further, by using the relation $I = 2\epsilon_o c|E|^2$ we may write

$$\Delta E = \pm \frac{|\langle j|\hat{\mu}|i\rangle|^2}{2\epsilon_o c\,\Delta} I \tag{4.24}$$

In the dipole approximation, the rate of spontaneous emission is given by

$$\Gamma = \frac{\omega_o^3 |\langle j|\hat{\mu}|i\rangle|^2}{3\pi\epsilon_o \hbar c^3} \tag{4.25}$$

Thus, the second order energy correction may be written in terms of the spontaneous emission rate, the intensity of the incident light field and its detuning from the atomic resonance ω_o:

$$\Delta E = \pm \frac{3\pi c^2}{2\omega_o^3} \frac{\Gamma}{\Delta} I \tag{4.26}$$

The energy shift due to the incident light field corresponds exactly to the dipole potential derived previously.

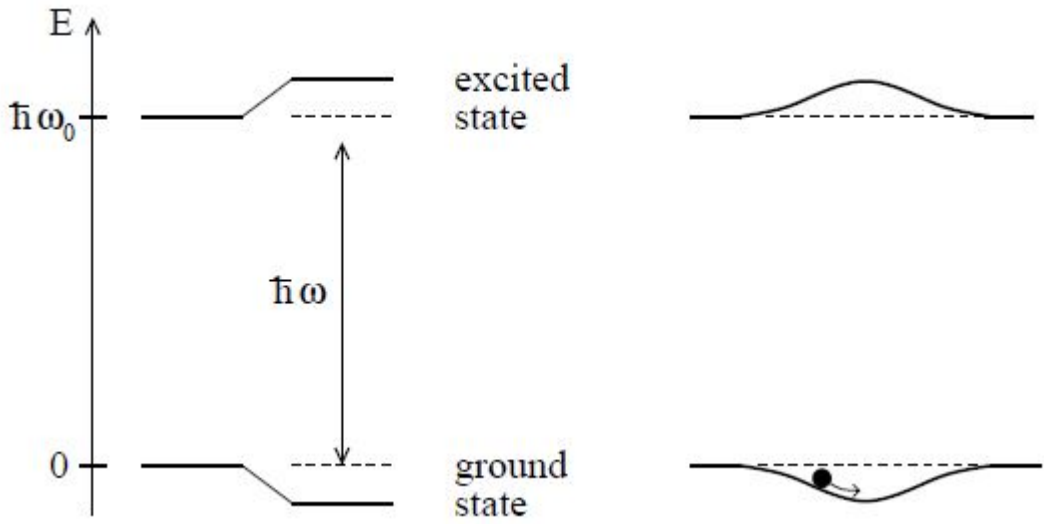

Fig. 4.1: (From [10]) Light shifts for a two-level atom. Left-hand side, red-detuned light ($\Delta < 0$) shifts the ground state down and the excited state up by equal amounts. Right-hand side, a spatially inhomogeneous field such as a Gaussian laser beam produces a ground-state potential well in which an atom can be trapped.

The shift in the energy levels of the atom resulting from an incident light field is known as the ac Stark shift. The detuning of the incident laser then allows for two classes of optical dipole traps: red-detuned and blue-detuned traps. In the case of red-detuning, the minima of the dipole potential are located where intensity is at a maximum and atoms are attracted into the light field. For the case of blue-detuning the opposite is true: the minima of the dipole potential are located where the intensity is at a minimum and atoms are repelled out of the light field [12]. For a red-detuned incident laser field, $\Delta < 0$, the ground state energy is shifted downwards while the excited state energy is shifted upwards, as shown in Figure 4.1. In experiments with low saturation, the atom spends most of its time in the ground state of the system and the motion

of the atoms can be considered to be governed by the down shifted ground state potential [13].

4.2.3 AC Stark Shift for Multi-level Atoms

Above we looked at the case of a two level system. If we extend our parameters to include an atom with multiple levels, the dipole matrix elements

$$\hat{\mu}_{ij} = \langle e_i|\hat{\mu}|g_i\rangle \tag{4.27}$$

between the allowed transitions from electronic ground and excited states must be determined. We can rewrite the dipole matrix elements in the form

$$\hat{\mu}_{ij} = c_{ij}||\hat{\mu}||, \tag{4.28}$$

where $||\hat{\mu}||$ is directly related to the spontaneous decay rate Γ, and c_{ij} is related to the coupling strength between the ground and excited states, the electronic and nuclear angular momentum, and the incident laser's polarization. Then, the total energy shift of the ground state in a multilevel system is given by

$$\Delta E = \frac{3\pi c^2}{2\omega_o^3}\Gamma I \times \sum_j \frac{c_{ij}^2}{\Delta_{ij}} \tag{4.29}$$

4.2.4 Alkali Atoms

Alkali atoms are prevalent in many experiments involving laser cooling and trapping due to their closed optical transitions that lie in a convenient spectral range. We will now consider the $n\,s \rightarrow n\,p$ transition for an alkali atom of nuclear spin $\mathbf{I = 3/2}$ shown in Figure 4.2. The fine structure splitting of the p state is written Δ'_{FS}, while the hyperfine structure splittings of the s and p states are Δ_{HFS} and Δ'_{HFS} respectively. The size of the energy splittings are such

that $\Delta'_{FS} \gg \Delta_{HFS} \gg \Delta'_{HFS}$.

In terms of total angular momentum $\mathbf{F = I + J}$, its magnetic quantum number m_F, and laser polarization P, the dipole potential is given as

$$\boldsymbol{U_{dipole}(r) = \frac{\pi c^2 \Gamma}{2\omega_0^3}\left(\frac{2 + P g_F m_F}{\Delta_{2,F}} + \frac{1 - P g_F m_F}{\Delta_{1,F}}\right) I(r).} \tag{4.30}$$

$\Delta_{1,F}$ is the energy splitting between $^2S_{1/2}$ and the center of the hyperfine split $^2P_{3/2}$, while $\Delta_{2,F}$ is the energy splitting between $^2S_{1/2}$ state and the center of the hyperfine split $^2P_{1/2}$ state. The laser polarization state is written as $\boldsymbol{P} = 0, \pm 1$ for linearly and circularly $\sigma^{\pm}$ polarized light, respectively, and g_F is the Lande factor. First we consider the case where the laser detuning is much larger than the fine structure splitting. Defining a detuning, Δ, relative to the regular center of the two transitions $^2S_{1/2} \rightarrow^2 P_{1/2}$ and $^2S_{1/2} \rightarrow^2 P_{3/2}$, and expanding the dipole potential, we find

$$\boldsymbol{U_{dipole}(r) = \frac{3\pi c^2}{2\omega_0^3}\frac{\Gamma}{\Delta}\left(1 + \frac{P g_F m_F}{3}\frac{\Delta'_{fs}}{\Delta}\right) I(r).} \tag{4.31}$$

The first term, however, is the same result obtained previously for a two-level atom (Eq. 4.18). Therefore we may conclude that if the fine structure of the atom is unresolved, then the atomic sublevels may be ignored and the transition reduces to a simple s $\rightarrow$ p transition.

4.3 Experimental Realization

4.3.1 Loading of Dipole Traps

The starting point for loading atoms into a dipole trap is to cool them in a MOT. Utilizing near-resonant light, MOTs are able to

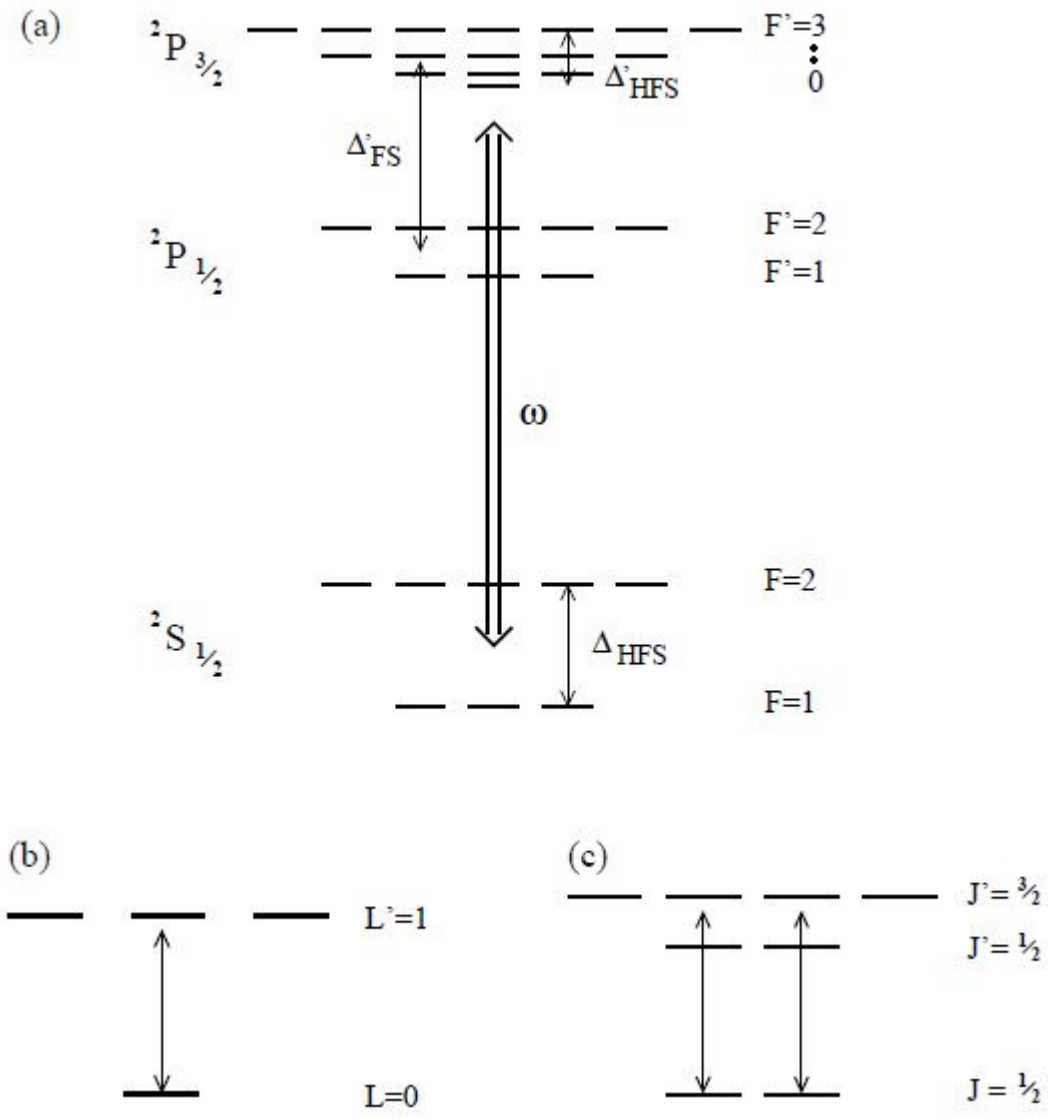

Fig. 4.2: (From [10]) (a) Full energy level diagram (including hyperfine splitting) for a nuclear spin I = 3/2 atom. (b) Reduced energy level diagram in the regime where $|\Delta| \gg \Delta'_{fs}$. (c) Reduced energy level diagram in the regime where $\Delta'_{fs} \geq |\Delta| \gg \Delta_{HFS}, \Delta_{HFS}$.

cool gases to several microKelvin starting from a thermal gas distribution. The MOT laser is first set to a small detuning from atomic resonance to maximize atomic capture by the resonant scattering force. This stage is then followed by the sub-Doppler cooling stage: the laser detuning is now set to a much greater value and then the laser intensity is reduced. Next, the magnetic fields of the MOT are switched off and the dipole trap is loaded simply by overlaying the trapping laser with the atomic cloud formed in the MOT. It is important to note that a red-detuned optical trap is beneficial for the loading process since with both the MOT and the dipole trapping laser active, the attractive dipole potential causes a localized increase in the atomic density of the MOT, providing greater efficiency in the loading of the dipole trap.

4.3.2 Red-detuned Dipole Traps

In the case of the red-detuned dipole trap, the dipole force pushes atoms in the direction of increasing light field intensity. Thus, the focus of the trapping laser beam serves as the potential with which atoms may be stably trapped. There are three major classes of trapping techniques that utilize red-detuning: focused beam traps which consist of a single beam, standing wave traps in which atoms are axially confined in the anti-nodes of a standing wave, and crossed beam traps where two or more lasers intersect at their foci.

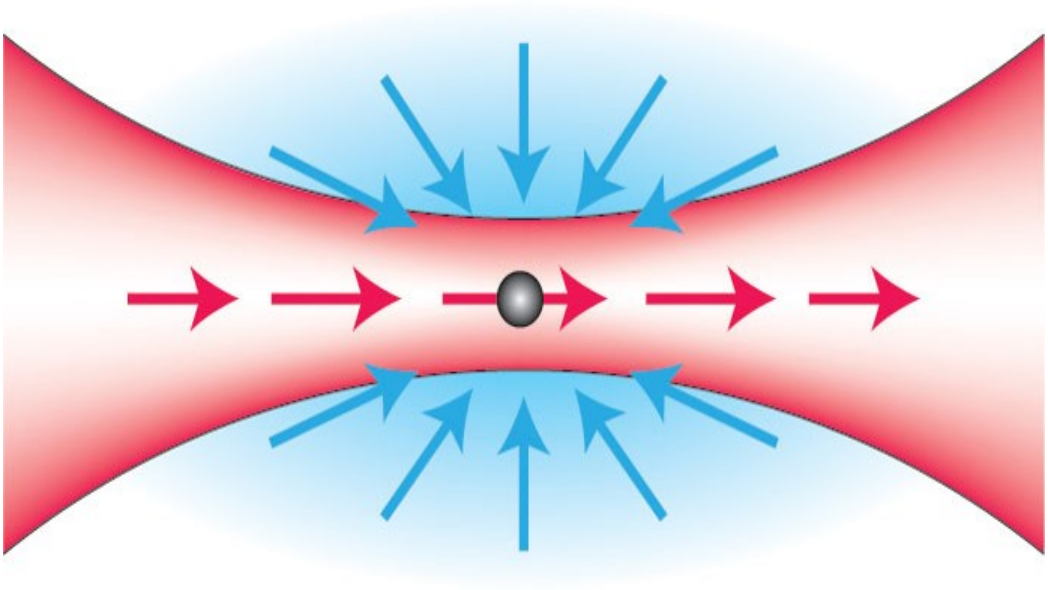

Fig. 4.3: (From [14]) Red-detuned dipole trap with atoms confined to the beam-waist of the trapping light.

4.3.3 Blue-detuned Dipole Traps

In the more complicated case of the blue-detuned dipole trap, the dipole force repels atoms away from the direction of increasing light field intensity. The process then is to fully enclose a spatial region with the repulsive laser light. Such a scheme minimizes the effects of photon scattering, light shifts of the atomic levels and light-assisted collisions. In contrast to red-detuned dipole trapping which can be achieved with a single focused laser beam, dipole trapping using blue-detuned laser light requires the construction of repulsive optical walls to confine the atoms. Like red-detuned traps, there are three major classes of trapping techniques: a strong elliptical focusing of a laser can produce light sheets, hollow lasers beams which allow for confinement in two or more dimensions, and evanescent waves produced by total internal reflection from

the surface of a dielectric medium. In blue-detuned traps it is also common to confine atoms from above by simply using gravity.

5. EXPERIMENTAL APPARATUS

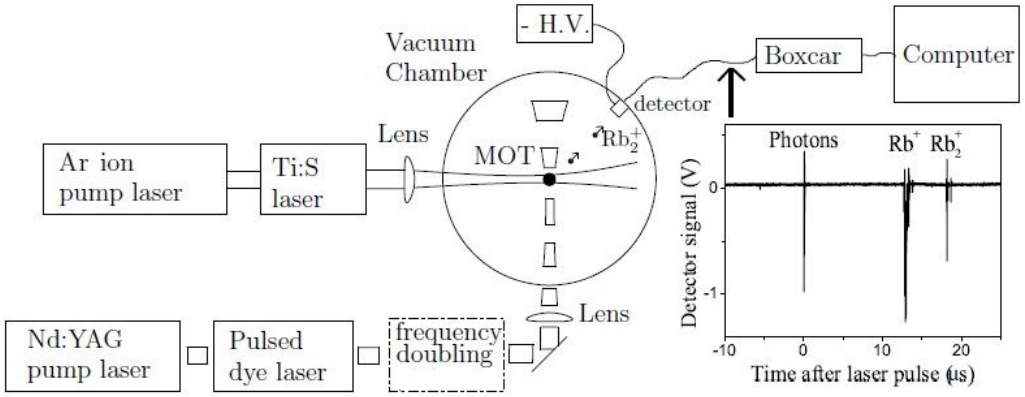

Fig. 5.1: (From [15]) Schematic of Rb_2 photoassociation from a MOT, pulsed autoionization and detection with a sample time of flight readout.

With our current apparatus the magneto-optical trap traps approximately $8*10^7$ atoms at a peak density of $1*10^{11}$ cm^{-3} at a temperature of 120 μK. A Ti:Sapphire laser continuously irradiates the MOT and converts a portion of the atoms into molecules via photoassociation. As shown in Fig. 5.2, the atoms form molecules in the (0_g^-) state which then radiatively decay to the $a\ ^3\Sigma_u^+$ state bound by -0.8 cm^{-1} below the 5s + 5s atomic asymptote. Molecules are continuously produced in the MOT, and are continuously lost because they are not trapped. The molecules that remain are periodically photoexcited with a pulsed amplifier chain operating in the uv at 365 nm. The uv laser beam utilizes a LDS750 dye solution and is pumped by a doubled Nd:YAG laser. Another frequency

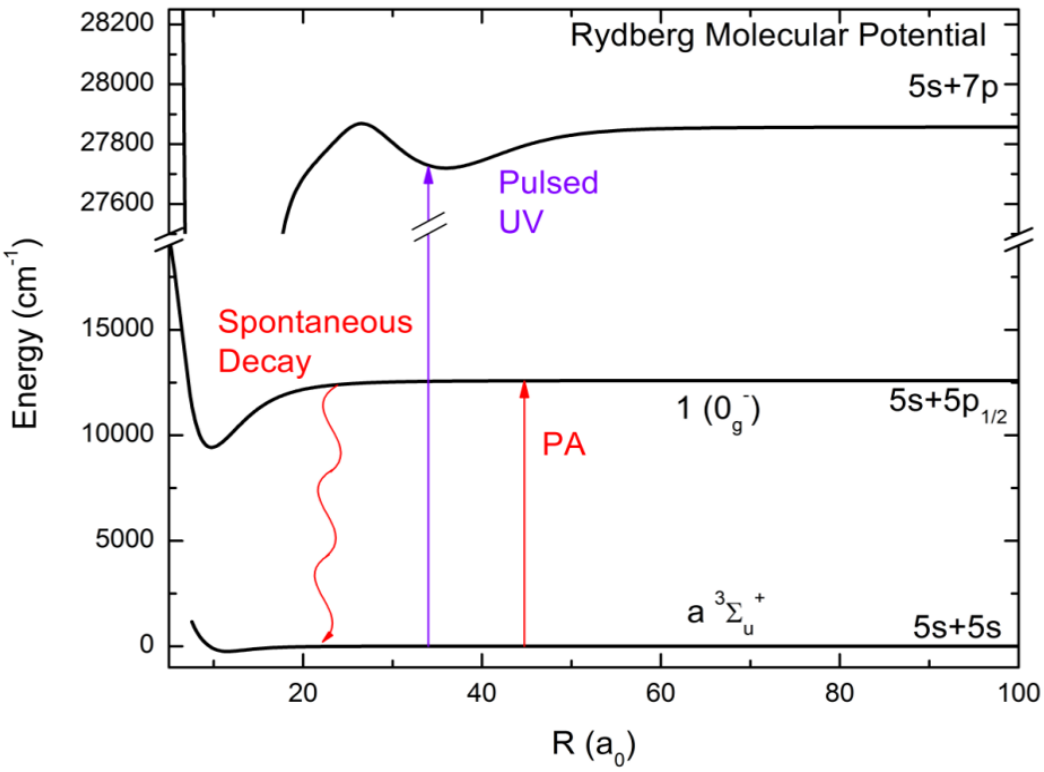

Fig. 5.2: (From [15, 16]) Rydberg 5s + 7p Rb_2 molecule formation pathway after pulsed UV formation of selected rovibrational levels of the $a\,^3\Sigma_u^+$ state by spontaneous decay following photoassociation to a selected rovibrational level of the $1(0_g^-)$ state from two free ultracold atoms trapped in a MOT.

doubler produces the second harmonic of the pulsed dye laser with roughly 25% efficiency, and the pulse energy is approximately 1 mJ/pulse [16]. When the molecules are excited to a Rydberg or trilobite state, they autoionize and an electric field plate accelerates atomic and molecular ions to a discrete dynode multiplier where the Rb^+ and Rb_2^+ ions are distinguished by their time of flight. A

boxcar integrator is used to determine the atomic and molecular ion signal.

6. TRIMER ION FORMATION

6.1 Enhanced Collisional Cross Section For Ultracold Rydberg Molecules

In [17] it was shown that the associative ionization ($Rb^{**} + Rb \rightarrow Rb_2^+ + e^-$) between a Rydberg rubidium atom Rb^{**} (p state, n = 30 - 60) and a ground-state rubidium atom possessed a scattering cross section three orders of magnitude larger than the geometrical size of the Rb_2^+ ion formed. The cross section enhancement relies on the Rydberg electron scattering off the ground-state atom, which attracts the ground-state atom towards the Rydberg atom ion core. Thus, the molecular ion forms when the ground-state atom's distance from the Rydberg ionic core is close enough such that, through the resonant dipole interaction, the Rydberg electron is ejected by the binding energy released to form the molecular ion. Further, the size of the electronic Rydberg wavefunction provides the limit for the inelastic collision cross section, since it was shown that the Rydberg excitation decayed for every ground-state atom that came within the electronic Rydberg wavefunction. It is important to note, however, that although there is an immense enhancement of the collisional cross section mediated by the Rydberg electron, the associative ionization to a molecular ion represents a rather small fraction of the reactions that occur. More often, the Rydberg atom itself decays, a neutral Rb_2 is formed, or

the Rydberg atom loses energy and ends in a lower excited state.

6.2 Alkali Trimers Formed on He Nanodroplets

Previous work [18] has performed excitation and emission spectroscopy on Na and K trimers formed on He nanodroplets, successfully resolving vibrational structure. Such work is subject to strong broadening of electronic spectra and suffers from lack of precision of ro-vibrational structure in comparison to gas-phase studies. However, the effects of spin-orbit coupling in triatomic species have been examined, with results that are pertinent to future work with homonuclear and heteronuclear triatomic species of Rb and K. The authors of [18] found that SO-coupling plays a significant role in the homonuclear case, enough to be critical for correct spectroscopic peak assignment, although proving to be negligible in the heteronuclear case. The cause of this disparity results from the reduced molecular symmetry, as discussed in [18]. Future studies in the gas-phase would thus benefit from understanding and further investigating the SO-coupling in both homo- and heteronuclear cases.

6.3 Extension to Triatomics

Energetics for reactions forming trimers of Rb and K were calculated and the energy level schematics are shown in Figures 6.1 and 6.2. There are two pathways that appear most promising for experimental studies in our current setup. The first involves exciting Rb_2 to a highly excited Rydberg state, Rb^{**}, from which it will react with neutral Rb atoms in the MOT to form $Rb_3^+ + e^-$. The other pathway involves a highly excited Rydberg Rb** atom which can collide with an Rb_2 molecule to form $Rb_3^+ + e^-$ via associative

ionization. In associative ionization the ejection of an electron is the mechanism which releases the binding energy necessary for the formation of a bound molecule [17]. In both trimer systems (rubidium and potassium), such collisions could occur for molecules excited to levels above the $Rb_3^+ + e^-$ and the $K_3^+ + e^-$ asymptotes, respectively; see Figures 6.1 and 6.2. The two pathways are shown below in equations 6.1 and 6.2, where A is either Rb or K.

$$\left\{ \begin{array}{l} \mathbf{A}_2 + h\nu_{Ryd} \rightarrow \mathbf{A}_2^{**} \\ \quad \mathbf{A}_2^{**} + \mathbf{A} \rightarrow \mathbf{A}_3^+ + e^- \end{array} \right\} \tag{6.1}$$

$$\left\{ \begin{array}{l} \mathbf{A} + h\nu_{Ryd} \rightarrow \mathbf{A}^* \\ \quad \mathbf{A}^* + \mathbf{A}_2 \rightarrow \mathbf{A}_3^+ + e^- \end{array} \right\} \tag{6.2}$$

Although the first process (6.1) is presumably occurs in our current experiment, it is a small percentage of the total ionization involved and has not been observed. We do, however, expect to observe an ionization cross section enhancement comparable to the dimer rubidium case explored in [17]. The same reaction that occurs between a Rydberg atom and a ground-state atom should similarly occur between a Rydberg dimer and a ground state atom (Eqn 6.2), leading to a bound trimer ion through associative ionization. To observe such reactions we must increase our atomic density in the MOT by at least a factor of one hundred via an optical dipole trap, the theoretical foundation and implementation of which is discussed in Chapter 4. To search for Rb_3^+ formation will require the installation of a third boxcar integrator that will monitor the detector output for time-of-flight signals, as is currently done for both the atomic and dimer signals. Since Rb^+, Rb_2^+ and Rb_3^+ possess the same electric charge, the differences in their masses will produce easily identified and unique time of flight spectra. If

Rb ions arrive at time t_{atoms} after the photons, then dimer Rb ions arrive at $t_{dimers} = \sqrt{2}\, t_{atoms}$ and the trimer Rb ions would arrive at $t_{trimers} = \sqrt{3}\, t_{atoms}$. Similar physics would also apply to K time-of-flight signals of course.

By constructing the optical dipole trap we will be able to reach colder atoms and denser samples. With such a trap in place we hope to observe Rb_3^+ spectra and enter a new experimental realm of ultracold trimer physics.

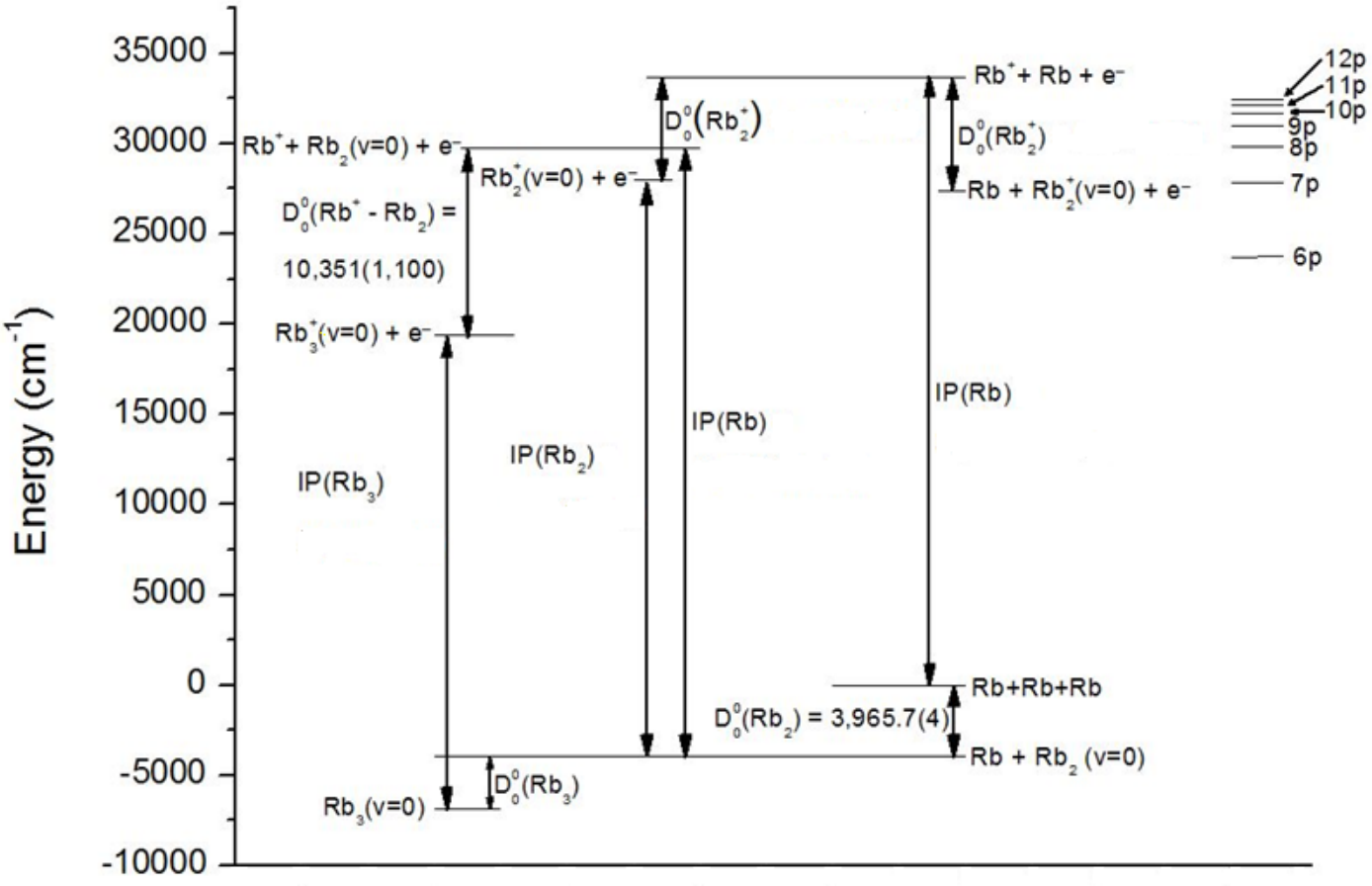

Fig. 6.1: (Data from [15, 19]) Energy level diagram for Rb atoms, dimers and trimers.

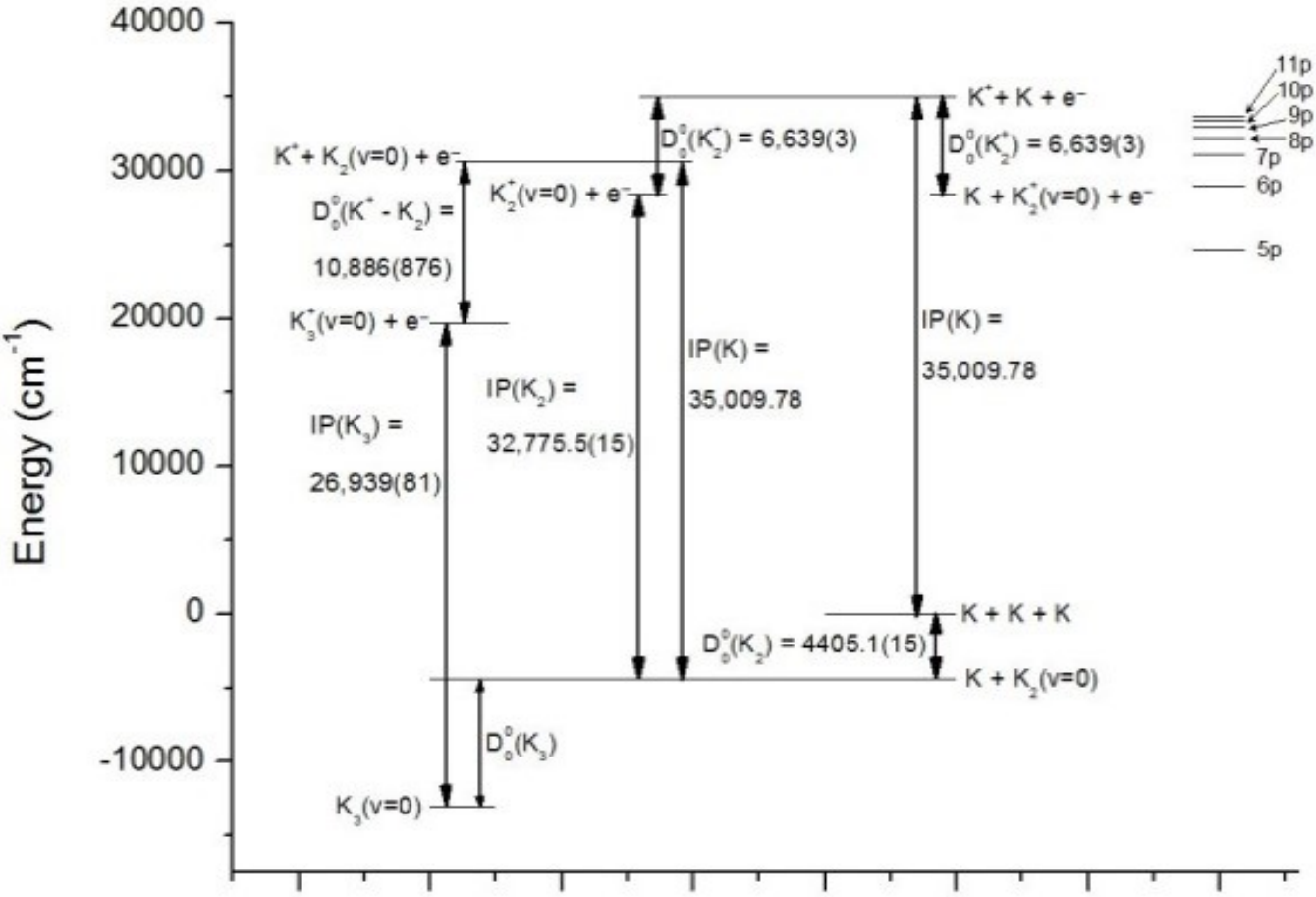

Fig. 6.2: (Data from [15, 19]) Energy level diagram for K atoms, dimers and trimers.

7. PROPOSAL FOR PHOTODISSOCIATION STUDIES IN OPTICAL LATTICES

In this section I propose to extend work done on photoassociation (PA) spectroscopy of ultracold diatomic molecules in an optical lattice. Optical lattices provide an interesting and unique framework for the study of ultracold collisional dynamics due to their highly ordered periodic confinement of atoms, a remarkable contrast to most collisional studies which take place in free space. Theoretical studies have been undertaken [20] to determine the effects that a 1D and 2D lattice potential will have on PA spectra, and recent work by the Zelevinsky group at Columbia has successfully experimentally realized a modified PA spectra in $^{88}Sr_2$ [21]. By extending this work to other diatomic molecules and optical lattices of diverse well depths and periodicities, I hope to provide a deeper understanding of collisional dynamics leading to molecule formation while augmenting theoretical *ab initio* quantum chemistry calculations. Photoassociation is the process where an electronically excited molecule is formed by the absorption of a resonant photon during the collision of two free atoms. Thus, a PA spectrum displays the number of molecules produced as a laser traverses a range of frequencies. In most PA spectra of alkali metals, Doppler broadening plays a minor role because transitions often occur to short-lived excited states [6]. With atoms prepared at ultracold temperatures, thermal broadening is minimal, and corre-

spondingly the range of initial kinetic energies is similar to the natural linewidth of the excited molecular state. Therefore, the PA of alkali metals provides high resolution spectra with linewidths only marginally larger than the natural linewidths. PA spectroscopy has led to the accurate measurement of radiative lifetimes for alkali metal atoms and provides binding energies relative to atomic asymptotes without requiring the extrapolation required in bound-bound spectroscopy.

Of particular interest is exploring the link between collisional processes and optical lattice dimensionality, as well as using optical lattices to perform high resolution photodissociation spectroscopy for the precise determination of molecular binding energies. Due to the relatively small trapping depth of optical dipole traps, preparing atoms in an optical lattice often requires the use of a magneto-optical trap (MOT). The operation of the MOT relies on the Doppler shift and the Zeeman splitting of the energy levels of the atoms to be cooled [9]. The approach is to confine a sample of the atomic species by passing three pairs of counter-propagating laser beams through the chamber, which is at ultra-high vacuum to insure only the atomic species of interest is present and to minimize collisions with any background gases. Once the ultracold cloud of atoms is formed in the MOT, an optical dipole trapping scheme is then implemented to further cool the atoms and increase the atomic density. The optical dipole trap relies on the force generated by an induced atomic dipole moment interacting with the intensity gradient of the incident light field. Atoms can be trapped in the derived potential, which is designed to have a periodicity resulting from the standing wave configuration of the trapping laser [10]. Such studies could prove a fruitful framework by providing much needed experimental data for collisions in opti-

cal lattices by studying systems of various trap depths and atomic species. An interesting aspect of this system worth exploring is the effect of a time-varying trap depth on both photoassociation and photodissociation spectra. Implementing such a scheme would require modulating the trapping laser power, a task well-suited for an acousto-optic modulator. A change in the trapping depth corresponds to a change in the energy of the trapped atoms. Thus, with the same excitation laser wavelength, one could photoassociate free atoms to a bound state, and then after varying the trap potential, excite the molecules to a state from which they photodissociate and return to free atoms. Such experiments could provide meaningful insight into optimal state transfer pathways for coherent control of molecular systems.

BIBLIOGRAPHY

[1] Roman Krems (Editor), Bretislav Friedrich (Editor), William C Stwalley (Editor), *Cold molecules: theory, experiment, applications*, CRC Press, (2009).

[2] M.A. Bellos, R. Carollo, J. Banerjee, E.E. Eyler, P.L. Gould, and W.C. Stwalley, Phys. Rev. Lett. 111, 053001 (2013).

[3] The 2001 Nobel Prize in Physics - Advanced Information. Nobelprize.org. Nobel Media AB 2014.

[4] J. Ye et al., Optics Express 18, 21861-21872 (2010).

[5] D. Leibfried *et al.*, Phys. Rev. Lett. 89, 247901 (2002).

[6] W.C. Stwalley and He Wang, J. of Mol. Spec. 195, 194228 (1999).

[7] V. Bendkowsky *et al.* Nature 458, 1005-1008 (2009)

[8] Chris H. Greene, A.S. Dickinson, and H.R. Sadeghpour, Phys. Rev. Lett. 85, 2458 (2000).

[9] J.F. Barry, D.J. McCarron, E.B. Norrgard, M.H. Steinecker and D. DeMille, Nature 512, 286289 (2014).

[10] R. Grimm, M. Weidemuller and Y. B. Ovchinnikov, Advances in Atomic, Molecular and Optical Physics 42, 95-170 (2000).

[11] **J. Dalibard and C. Cohen-Tannoudji, J. Opt. Soc. Am. B 2, 1707-1720 (1985).**

[12] **Matthias Schulz, PhD Thesis, Universität Innsbruck, 2002.**

[13] **Harold J. Metcalf and Peter van der Straten, J. Opt. Soc. Am. B 20, 887 (2003).**

[14] **Timo A. Nieminen, Nature Photonics 4, 737-738 (2010).**

[15] **M.A. Bellos, PhD Thesis, University of Connecticut, 2013.**

[16] **M.A Bellos, R. Carollo, J. Banerjee, M. Ascoli, A.-R. Allouche, E.E. Eyler, P.L. Gould, and W.C. Stwalley, Phys. Rev. A 87, 012508 (2013).**

[17] **T. Niederprüm, O. Thomas, T. Manthey, T.M. Weber, and H. Ott, Phys. Rev. Lett. 115, 013003 (2015).**

[18] **C. Giese, F. Stienkemeier, M. Mudrich, A.W. Hauser and W.E. Ernst, Phys. Chem. Chem. Phys 13, 18769-18780 (2011).**

[19] **W.C. Stwalley and J.T. Bahns, Laser and Particle Beams 11, 185-204 (1993).**

[20] **P. Naidon and P.S. Julienne, Phys. Rev. A 74, 062713 (2006).**

[21] **B.H. McGuyer et.al., New Journal of Physics 17, 055004 (2015).**